ADVANCED FUNCTIONAL MATERIALS

DOI: 10.1002/adfm.200800496

Effect of SWNT Defects on the Electron Transfer Properties in P3HT/SWNT Hybrid Materials**

By *Jianxin Geng, Byung-Seon Kong, Seung Bo Yang, Sang Cheon Youn, Sohyun Park, Taiha Joo,* and *Hee-Tae Jung**

Poly(3-hexylthiophene) (P3HT) hybrids with single-walled carbon nanotubes (SWNTs) were prepared using a series of SWNTs with various defect contents on their surfaces. The hybrids were synthesized by exploiting the π–π interaction between P3HT and the SWNTs, resulting in efficient dispersion of the carbon nanotubes in the P3HT solution. UV-visible and photoluminescence (PL) spectra showed that the carbon nanotubes quench the PL of P3HT in the hybrids, indicating that electron transfer occurs from photo-excited P3HT to the SWNTs. This electron transfer from P3HT to carbon nanotubes was disrupted by the presence of defects on the SWNT surfaces. However, the PL lifetime of P3HT in the hybrids was found to be the same as that of pure P3HT in solution, indicating the formation of a ground-state non-fluorescent complex of P3HT/SWNTs.

1. Introduction

Polythiophene and its derivatives have attracted considerable attention in recent years because of their potential applications in polymer-based light emitting diodes (PLED), field-effect transistors (FETs), polymer solar cells, and sensors.[1–4] Polythiophenes emit orange-red light, consistent with their band gap of around 2 eV. Emission in this wavelength range is difficult to achieve with other conjugated polymers,[5] making polythiophenes particularly attractive candidates for PLED display applications. The photoluminescence (PL) efficiency of polythiophenes in the solid state is much lower than that in solution[5,6] due to the enhanced contribution of non-radiative decay via the stronger interchain interactions in the solid state and intersystem crossing caused by the heavy-atom effect of sulfur.[7] This feature is an advantageous characteristic of polythiophenes for their potential application in FETs and polymer solar cells. Indeed, the polymer solar cells with the highest efficiency reported to date were based on a combination of poly(3-hexylthiophene) (P3HT) and fullerene derivatives.[8] Moreover, it is feasible to modulate the band-gap and energy level of the highest occupied molecular orbital (HOMO) of polythiophene derivatives through molecular design in order to make a polymer whose absorption matches the maximum photon flux of the solar spectrum and to improve the photo response voltage.[3a,9]

Hybridization of polythiophene and functional nanomaterials usually enhances the combined attributes of each component such as conducting properties, optical properties, and donor-acceptor properties.[10] In such hybrid materials, electron transfer between the polythiophene and the other component, which usually functions as an electron acceptor (e.g., fullerene, inorganic nanoparticles, and conjugated polymers having higher electron affinity than P3HT), plays an important role in determining the performance of the photovoltaic device.[11] Recently, it has been verified that complexes of polythiophene and carbon nanotubes (CNTs) are strong candidate materials for photovoltaic device applications because SWNTs can act as both electron acceptors and electron transportation paths.[12] Furthermore, the inclusion of SWNTs can improve the morphology and increase the crystallinity of the active layer, thereby enhancing solar cell performance.[12a] If P3HT/SWNT hybrids are to be used in molecular electronics such as photovoltaics, it is important to understand the electron transfer behavior in these hybrids.

In this study, we demonstrate that P3HT and SWNTs constitute a donor-acceptor system, which is expected to be a promising candidate to form optically active materials for photoelectronics applications. We show that the addition of SWNTs to a P3HT solution quenches the PL of P3HT, reflecting electron transfer from photoexcited P3HT to the

[*] Prof. H.-T. Jung, Dr. J. Geng, B.-S. Kong, S. B. Yang, S. C. Youn
Department of Chemical and Biomolecular Engineering (BK-21)
Korea Advanced Institute of Science and Technology
373-1 Guseong-dong, Yuseong-gu, Daejeon 305-701 (Korea)
E-mail: heetae@kaist.ac.kr
S. Park, Prof. T. Joo
Department of Chemistry
Pohang University of Science and Technology
Pohang, 790-784 (Korea)

[**] This work was supported by the National Research Laboratory Program of the Korea Science & Engineering Foundation (KOSEF), the Center for Nanoscale Mechatronics & Manufacturing (CNMM), and the Blue Ocean Program of Small and Medium Business Administration. We thank Dr. Dan Zhao in the Department of Material Sciences and Engineering at KAIST for helpful discussions. Supporting Information is available online from Wiley InterScience or from the authors.

SWNTs. Moreover, we demonstrate that the electron transfer efficiency from P3HT to SWNTs is strongly influenced by the SWNT defect content. This work furthers our understanding of the interaction between conjugated polymers and CNTs, thereby facilitating the application of poly(3-alkylthiophene)/SWNT systems in molecular electronics.

2. Results and Discussion

P3HT was non-covalently hybridized with SWNTs having various defect contents: (i) AP-SWNTs (as-prepared SWNTs), (ii) P1-SWNTs (purified SWNTs with air oxidation at 300 °C for 1 hour and HCl washing for 2.5 hours), (iii) P2-SWNTs (purified SWNTs subjected to two cycles of air oxidation and HCl washing), (iv) C1-SWNTs (cut SWNTs with piranha solution oxidation for 2 hours), (v) C2-SWNTs (cut SWNTs with piranha solution oxidation for 4 hours). The defects were produced in the purification process or deliberately generated by oxidation with piranha solution, where the defect content was controlled by varying the oxidation time (Scheme 1a). The relative amounts of SWNT defects were estimated by measuring the variation in the D-band (frequency $\sim 1350\,cm^{-1}$) and G-band (frequency $\sim 1582\,cm^{-1}$) in the Raman spectra (Fig. 1). Notable changes in the D-band of the purified and piranha-solution-treated SWNTs with respect to the AP-SWNTs were observed, indicating that a large structural modification of the SWNT sidewalls is induced by the introduction of defects. The D-band feature stems from a disorder-induced mode in graphite; therefore, changes in the D-band can be used to monitor changes in defect density in nanotube sidewalls.[13] The intensity of the D-band in Raman spectra increases gradually as the purification and piranha solution oxidation proceed, indicating that the SWNT samples have different defect contents: AP-SWNTs ($I_D/I_G \sim 0.10$, where I_D and I_G represent the intensities of the D-band and the G-band in Raman spectra, respectively) < P1-SWNTs ($I_D/I_G \sim 0.14$) < P2-SWNTs ($I_D/I_G \sim 0.18$) < C1-SWNTs ($I_D/I_G \sim 0.21$) < C2-SWNTs ($I_D/I_G \sim 0.21$). Scheme 1b shows that the P3HT/SWNT hybrid is formed through polymer wrapping of P3HT around SWNTs.[14]

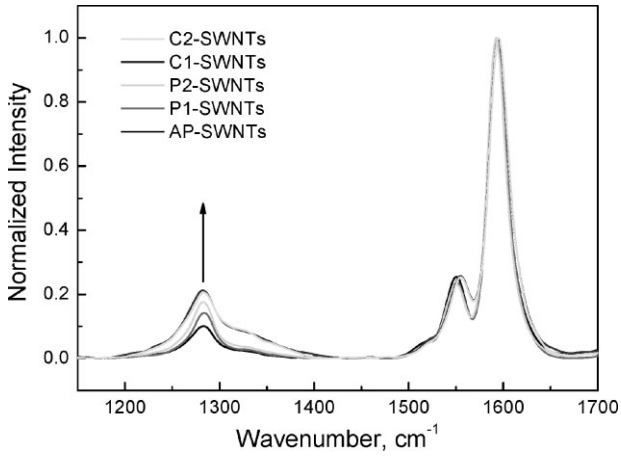

Figure 1. Raman spectra of a series of SWNTs.

The solubility of the P3HT/P1-SWNT hybrids in chloroform was observed by visual inspection (Fig. 2) and transmission electron microscopy (TEM) (Fig. 3). The color of the P3HT solution in chloroform changes from orange (Fig. 2a) to brown immediately after the P1-SWNT suspension is added because of the superposition of the optical absorptions of P3HT and the SWNTs. The solution color gradually intensifies during the sonication process, and the resultant dark brown solution (Fig. 2c) is more stable than the P1-SWNT suspension (Fig. 2b) because no precipitate was observed after the P3HT/P1-SWNT hybrid solution was kept standing for weeks, indicating that the uniform dispersion of CNTs with the aid of sonication results from the non-covalent interaction between CNTs and P3HT molecules. This result is consistent with the solubilization effect of other conjugated polymers.[15,16] Similar solution behaviors were observed for the other P3HT/SWNT hybrids: P3HT/AP-SWNTs, P3HT/P2-SWNTs, P3HT/C1-SWNTs, and P3HT/C2-SWNTs. It is noteworthy that a small amount of precipitate was observed at the bottom

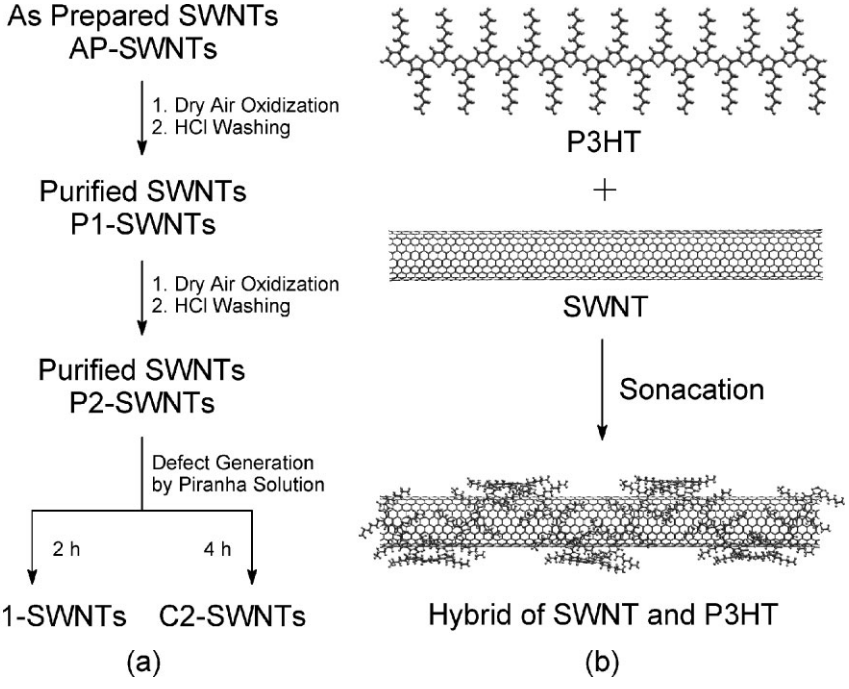

Scheme 1. A schematic illustration of the preparation of P3HT/SWNT hybrids.

ADVANCED FUNCTIONAL MATERIALS

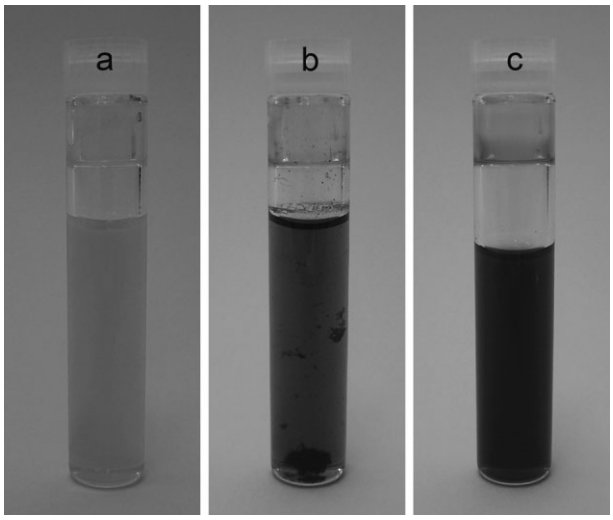

Figure 2. Optical images of a) P3HT solution in chloroform, b) P1-SWNT suspension in chloroform, and c) P3HT/P1-SWNT hybrid solution in chloroform.

of the P3HT/AP-SWNT hybrid solution after the solution was kept standing for several days. This precipitate may be amorphous carbon because the conjugated polymers show preferential interaction with SWNTs over amorphous carbon.[15,16] To simplify the description of experiments and the corresponding discussion, we select P1-SWNTs as an example, and then extend the conclusions to the other SWNT samples to investigate the effect of the defects on the properties of the P3HT/SWNT hybrids.

TEM images of films of the P3HT/P1-SWNT hybrids further confirm the efficient dispersion of the SWNTs in the P3HT solution (Fig. 3). TEM images show that the P1-SWNTs in chloroform aggregate densely (Fig. 3a), whereas the P3HT/P1-SWNT hybrids exhibit a uniform film (Fig. 3b), supporting the finding that the P1-SWNTs are homogeneously dispersed in the P3HT solution. Close observation of the films further confirms that the P1-SWNTs dispersed in P3HT solution exhibit thinner bundles than those in chloroform (inset of Fig. 3). The P3HT/SWNT hybrids formed with the other SWNTs having different defect contents, namely the P3HT/AP-SWNTs, P3HT/P2-SWNTs, P3HT/C1-SWNTs, and P3HT/C2-SWNTs, show similar solution behaviors to the P3HT/P1-SWNT system. It is likely that the interaction between P3HT and SWNTs via π-stacking overcomes the van der Waals interaction between CNTs, resulting in debundling of the CNTs. Thus, the SWNTs dispersed in the P3HT solution exist in very small bundles, or even as isolated tubes.

The optical absorption, PL, and emission quenching behaviors of the P3HT/P1-SWNT hybrids were studied using UV-visible spectroscopy and fluorophotometry (Fig. 4). Figure 4a shows the optical absorption spectra of P3HT/P1-SWNT hybrids with a P3HT concentration of 0.02 $mg \cdot ml^{-1}$ and an SWNT-to-P3HT concentration ratio varying from 0 to 2 (Table 1). The background increases with the P1-SWNT concentration due to the scattering effect of the nanotubes in the solutions.[17] The spectrum of the P3HT solution contains an absorption maximum at 449 nm that is attributed to electron transition from the HOMO to the lowest unoccupied molecular orbital (LUMO) of the polymer. The spectra of the P3HT/P1-SWNT hybrids contain absorption peaks corresponding to both P3HT and CNTs: the absorption peak at 449 nm is attributed to P3HT; the absorption peaks in the range of 500 nm to 900 nm are ascribed to the second van Hove transition of semi-conducting CNTs (E_{22}^{S}); and the new absorption peaks below 450 nm derive from the first van Hove transition of metallic CNTs (E_{11}^{M}). It has been established that the interaction between conjugated polymers and CNTs takes place via polymer wrapping around the CNTs or parallel adhesion of the polymer main-chains to the nanotube surfaces, depending on the stiffness of the polymer backbone and the length of the polymer chains; such π–π interactions between conjugated polymers and CNTs usually result in band shift or broadening of the polymers' characteristic absorption peaks due to the change of the effective conjugation length of the conjugated polymer in the presence of nanotubes.[15c,18] The characteristic absorption peak at 449 nm arising from P3HT is broadened in the spectra of the hybrids compared with the spectrum for pure

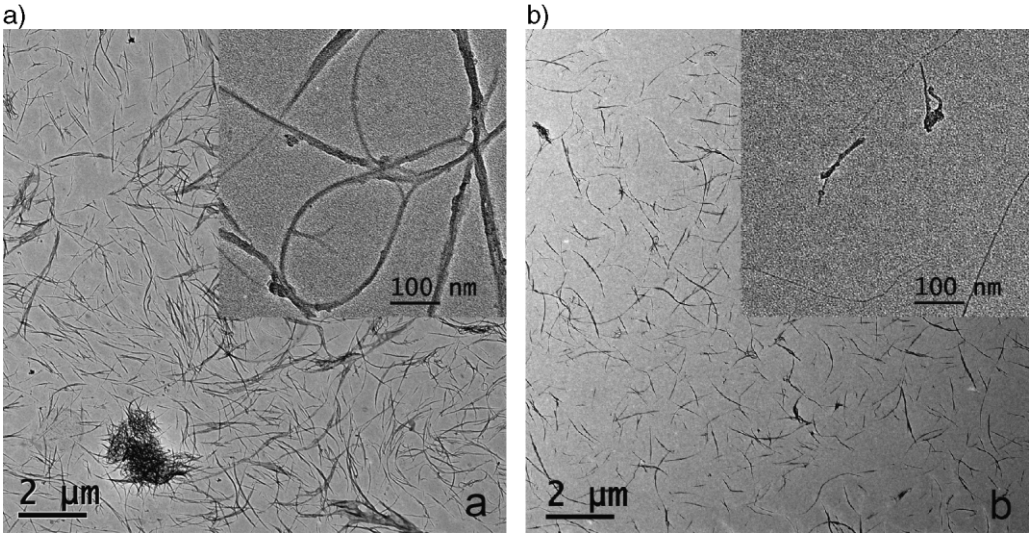

Figure 3. TEM images of a) P1-SWNTs obtained from its suspension in chloroform and b) P1-SWNT obtained from its suspension in P3HT solution. The inset shows the corresponding P1-SWNTs at high magnification.

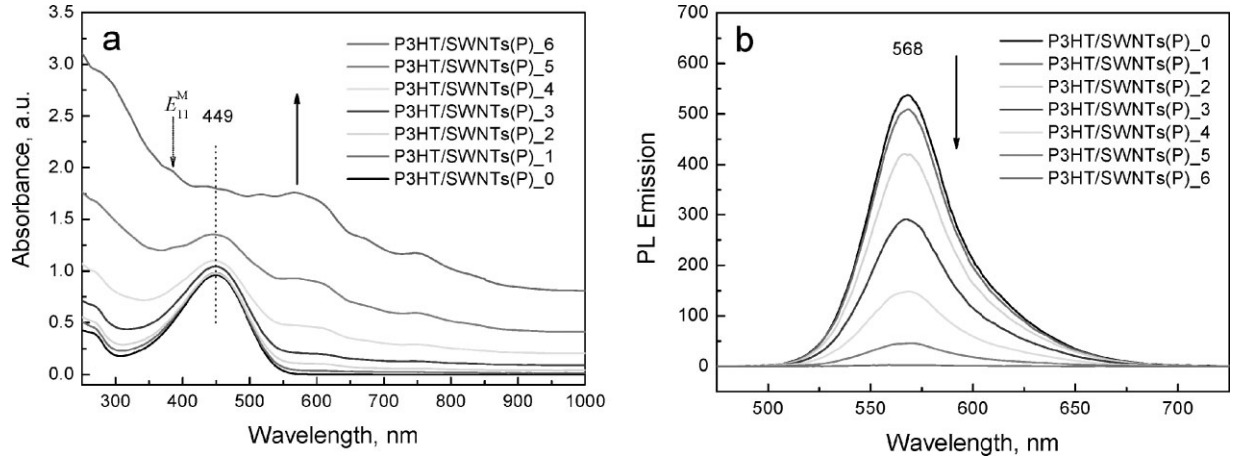

Figure 4. a) Optical absorption spectra and b) PL emission of a series of P3HT/P1-SWNT hybrid solutions in chloroform.

P3HT (Fig. 4a), consistent with a π–π interaction between the P3HT and the CNTs in the hybrids. The P3HT hybrids formed with the other SWNT samples (AP-SWNTs, P2-SWNTs, C1-SWNTs, and C2-SWNTs) provide similar optical absorption results to those for the P1-SWNTs, except that the absorption spectra in the materials with higher defect contents contain weaker absorption peaks corresponding to the van Hove transition of CNTs (Supporting Information, Fig. S1), indicating that the defects interrupt the efficient interaction between the P3HT molecules and the CNTs.

We found that the SWNTs quench the PL of P3HT, and that the quenching behavior of the CNTs is strongly influenced by the SWNT concentration (Fig. 4b) and defect content. P3HT and the P3HT/SWNT hybrids yield PL spectra with maximum emission peaks at 568 nm, which corresponds to the onset of the HOMO-LUMO transition of P3HT in the UV-visible absorption curve.[19] The P3HT/P1-SWNT hybrids yield weaker PL than pure P3HT, with the PL intensity decreasing with increasing CNT concentration; these findings are consistent with quenching of the PL of P3HT by the CNTs. The quenching of the P3HT PL when P3HT is exposed to CNTs implies that there is a process that is competing with the radiative emission of P3HT in the P3HT/P1-SWNT hybrids. A process that would account for the observed quenching is charge transfer from the LUMO band of the P3HT to CNTs. Our observation of more effective quenching by CNTs with higher nanotube concentrations is consistent with this mechanism, given that the rate of electron transfer from photo-excited P3HT to SWNTs will be affected by the interfacial area between P3HT and CNTs.

To quantitatively estimate the quenching efficiency of the SWNTs in the hybrid materials, we define the following quenching efficiency parameter:

$$\eta = 1 - \frac{\frac{I_i}{A_i}}{\frac{I_0}{A_0}} = 1 - \frac{I_i \cdot A_0}{A_i \cdot I_0} \quad (1)$$

where A_0 and A_i represent the absorbance at the wavelength that is used to excite the samples in the absence and presence of CNTs, and I_0 and I_i represent the integral of the PL emission in the absence and presence of CNTs, respectively. Table 1 summarizes the rectified absorbance (i.e., the maximal absorbance after subtracting the baseline derived from SWNT scattering), the integral of PL emission, and the quenching efficiency in detail for each of the P3HT/P1-SWNT hybrids.

Table 1. Concentration ratio and quenching efficiency of a series of P3HT/P1-SWNT hybrids.

No.	Ratio of P1-SWNTs to P3HT	Concentration Ratio	Absorbance (*A*)[a]	Integral of PL Emission (*I*)	*I*/*A*	Quenching Efficiency (η)
0	0:2	0	0.963	30616	34298	0
1	0.1:2	0.05	0.952	28919	30385	0.114
2	0.2:2	0.1	0.938	24177	25776	0.248
3	0.5:2	0.25	0.953	16935	17770	0.482
4	1:2	0.5	0.895	8832	9862	0.712
5	2:2	1	0.940	2773	2951	0.914
6	4:2	2	0.987	151	153	0.996

[a]The maximal absorbance is rectified by subtracting the baseline derived from SWNT scattering.

Figure 5 shows the change in the quenching efficiency of SWNTs as a function of the SWNT-to-P3HT concentration ratio for the SWNTs with different defect contents. The quenching efficiency curve for the P3HT/P1-SWNT hybrid can be divided into two concentration ratio ranges: a linear increase when the P1-SWNT-to-P3HT concentration ratio is less than 0.5, and a plateau region for concentration ratios greater than 0.5. For example, the cross-over between the linear and plateau regimes occurs at a P1-SWNT-to-P3HT concentration ratio of 0.5, which may arise from the optimal solubilization effect of P3HT on P1-SWNTs. When the concentration ratio is less than 0.5, P3HT can provide effective dispersion of P1-SWNTs, i.e., the P1-SWNTs can be efficiently

ADVANCED FUNCTIONAL MATERIALS

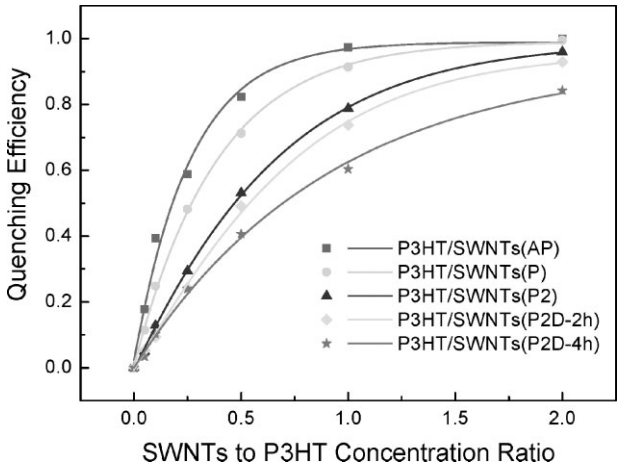

Figure 5. The change of quenching efficiency as a function of the SWNT-to-P3HT concentration ratio for each SWNT hybrid.

dispersed in P3HT solution. Therefore, the interfacial area between P3HT and the P1-SWNTs increases linearly with the P1-SWNT content in the hybrids when the concentration ratio is less than 0.5; as a result, the electron transfer between photoexcited P3HT and P1-SWNTs, resulting in PL quenching, increases linearly with the P1-SWNTs content. On the other hand, when the concentration ratio is greater than 0.5, P3HT loses the effective dispersion of P1-SWNTs, i.e., addition of more P1-SWNTs into the P3HT/P1-SWNT hybrid solution will not lead to an increase in the interfacial area between P3HT and the CNTs; as a result, the quenching efficiency remains constant. Thus, these results suggest that maximal dispersion of the P1-SWNTs in P3HT occurs at a concentration ratio of P1-SWNTs:P3HT = 1:2 for the concentration range considered in the present study. The quenching efficiencies for the other hybrids as a function of the SWNT-to-P3HT concentration ratio are also shown in Figure 5. These samples exhibit the same behavior as the P1-SWNT hybrids, namely a linear increase at low concentration ratio and a plateau at high concentration ratio.

We found that at a given concentration ratio, the quenching efficiencies differed among the various hybrid samples: AP-SWNTs > P1-SWNTs > P2-SWNTs > C1-SWNTs > C2-SWNTs. In addition, we found that the cross-over points for the SWNTs became undistinguishable at higher defect contents. These findings can be ascribed to the influence of defects on the π–π interaction between P3HT and the CNTs. It is likely that the presence of defects on the CNT surfaces disturbs the effective interaction of the SWNTs with P3HT. The above order of the materials in terms of decreasing quenching efficiency is the opposite of the sequence in terms of defect content obtained from Raman spectroscopy measurements: AP-SWNTs < P1-SWNTs < P2-SWNTs < C1-SWNTs < C2-SWNTs. This is consistent with a picture in which a more perfect CNT surface allows more efficient interaction between the nanotube and P3HT main-chains.

P3HT main chains can readily and uniformly wrap around CNTs with perfect surfaces. However, when the P3HT backbones pass through regions with defects, the interaction between P3HT and the nanotubes becomes weaker due to diminished π–π interactions. Therefore, when SWNTs are covered with P3HT molecules, the effective interfacial area corresponding to π–π interaction will be higher for SWNTs with fewer defects. As a result, the saturated quenching efficiency of the SWNT samples decreases with increasing defect content, with the highest quenching efficiency being observed for the AP-SWNTs (Fig. 5).

To further estimate the quenching mechanism, the PL quenching characteristics of P3HT by SWNTs were analyzed using the Stern–Volmer (SV) relation.[20] Figure 6a shows the variation of I_0/I as a function of the SWNT concentration C, where I_0 and I are the steady-state PL intensities in the absence and presence of SWNTs, respectively, and C represents the weight concentration of the SWNTs in the hybrid solutions. The SV plots are linear at low concentration, with positive deviations at high concentration. To further investigate the quenching behaviors of SWNTs, the PL lifetimes of P3HT in the absence and presence of SWNTs were measured using time

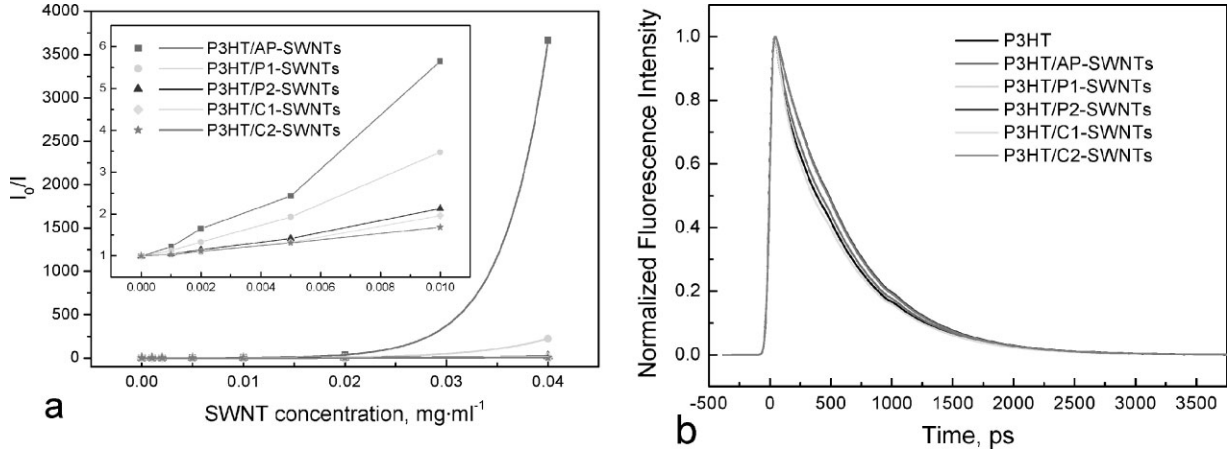

Figure 6. a) Stern–Volmer plots for the P3HT/SWNT hybrids, and b) lifetime profiles of P3HT in the absence and presence of carbon nanotubes.

resolved photoluminescence spectroscopy (Fig. 6b). The pure P3HT solution in chloroform was found to have a PL lifetime of 500 ps,[21] and its hybrids with SWNTs showed the same PL decay as the pure P3HT solution. Based on the observation that the PL lifetime profiles of the P3HT/SWNT hybrid solutions are the same as that of the P3HT solution, albeit with significantly lower PL intensities (Fig. 4b), we conclude that P3HT and SWNTs form a ground-state complex that does not luminesce. That is, the PL of the P3HT/SWNT hybrid solutions derives from the free P3HT, whereas the P3HT molecules hybridized with SWNTs do not contribute to the PL. Generally, when C60 or SWNTs quench the PL of fluorescent materials such as conjugated polymer, conjugated organic molecule, and quantum dots, the PL lifetime tends to decrease as the C60 or SWNT concentration increases.[22] The shortening of the PL lifetime derives from the electron transfer from the excited state to the quencher (C60 or SWNTs), which is competitive with the intrinsic decay from the excited state to the ground state of the fluorescent materials. However, in this study, the PL lifetime of P3HT/SWNT hybrids is the same as that of neat P3HT due to the formation of ground-state non-fluorescent complex.

In the case of the formation of a ground-state non-fluorescent complex, the relationship between I_0/I and the quencher concentration follows the equation,[20]

$$\frac{I_0}{I} = 1 + K_S \cdot [Q] \tag{2}$$

where K_s is the stability constant of the ground-state non-fluorescent complex and [Q] is the concentration of the quencher. The P3HT/SWNT hybrids are formed via π–π interaction, and the defects on the surfaces of the CNTs will disrupt the effective interaction of the SWNTs with P3HT. Therefore, the effective concentration of the quencher is controlled by the defect content. In this case, Equation 2 can be modified to

$$\frac{I_0}{I} = 1 + K_S \cdot \alpha \cdot C \tag{3}$$

where α represents the ratio of the SWNT surface area without defects to the total SWNT surface area, and C represents the weight concentration of SWNTs in the hybrid solutions. Figure 6a shows that the AP-SWNTs exhibit the highest slope, whereas the SWNTs with higher defect contents display lower slopes, consistent with the interpretation that the SWNT defects disrupt the π–π interaction between P3HT and the nanotubes, thereby reducing the electron transfer.

3. Conclusions

We have systematically studied the solubilization of SWNTs in P3HT solution and the effect of CNT defects on electron transfer from photoexcited P3HT to SWNTs. SWNTs were efficiently dispersed in the P3HT solution, resulting in the formation of non-covalent P3HT/SWNT complexes. Optical absorption spectroscopy, steady-state PL spectroscopy, and PL lifetime measurements showed that the SWNTs quench the PL from P3HT in the P3HT/SWNT hybrids. The results further indicated that defects on the CNT surfaces markedly disrupt electron transfer from photoexcited P3HT to the SWNTs. The present results deepen our understanding of the electronic properties of hybrids formed between conjugated polymers and CNTs, and should facilitate the application of polythiophene/SWNT systems in molecular electronics.

4. Experimental

Materials: The SWNTs (HiPco) used in this study were purchased from Carbon Nanotechnologies Inc. P3HT (MW 87,000 $g \cdot mol^{-1}$) was obtained from Aldrich, and its regioregularity was greater than 98.5% head-to-tail regiospecific conformation. All other chemicals (extra purity grade) were obtained from Junsei Chemical Co. Ltd.

Preparation of P3HT-SWNT Hybrids: Scheme 1 shows the overall process for fabricating P3HT-SWNT hybrids via the ultrasonication method, using a series of SWNT samples with various defect contents. As-prepared SWNTs (AP-SWNTs) were purified by dry oxidization at 300 °C for 60 min in a flow of dry air (0.1 SLM) and acid oxidation in 12 N HCl solution [23]. It is generally believed that amorphous carbon is removed during the dry oxidization process, and, importantly, that carbon coating on the metal particles is weakened during this step, followed by etching of the catalyst in the acid oxidation step. To purify the sample as much as possible, the dry air oxidation and acid oxidation were repeated once. Defects on the SWNT surfaces were deliberately generated by treatment with piranha solution (H_2SO_4:H_2O_2 = 4:1 in volume) at room temperature, with the defect content controlled by adjusting the treatment time [24]. The samples at each step were characterized with thermogravimetric analysis and Raman spectroscopy to probe the catalyst amount and defect content. The catalyst amount was determined to be 17.2% for AP-SWNTs, 6.9% for P1-SWNTs, 5.3% for P2-SWNTs, and less than 5% for the piranha solution treated samples, C1-SWNTs and C2-SWNTs. P3HT and SWNTs were separately dissolved and dispersed in chloroform, with the aid of sonication for the SWNT case. Designated amounts of P3HT solution and SWNT suspension were mixed and sonicated to obtain the hybrids of P3HT and SWNTs with various concentration ratios.

Characterization: Raman spectra were recorded on a Bruker RFS-100 Raman Spectrometer with an excitation wavelength of 1064 nm. Five hundred spectra were obtained for each sample and averaged in order to increase the signal to noise ratio. Powder-type samples were used for the Raman spectroscopy measurements. TEM observation was performed using a JEOL JEM-2100F instrument operated at 200 kV. TEM samples were prepared by dropping the SWNT suspension or the hybrid solutions on 400 mesh copper grids with supporting carbon film. UV-visible spectra were recorded with a JASCO V-570 spectrophotometer. Steady-state PL spectra were obtained using a Shimadzu RF-5301 PC spectrofluorophotometer with an excitation wavelength of 450 nm.

PL life time profiles of the P3HT and P3HT/SWNT hybrids were obtained by the time correlated single photon counting (TCSPC) method. Output of a home-built cavity-dumped Kerr lens mode-locked Ti:sapphire laser running at 820 nm was doubled to generate excitation pulses at 410 nm. Fluorescence at the magic angle was detected by a thermoelectrically cooled microchannel plate photomultiplier tube (Hamamatsu, R3809U-51). The instrument response function had a full width at half maximum of 42 ps to provide ~8 ps time resolution

ADVANCED FUNCTIONAL MATERIALS

with deconvolution. A sample cuvette was attached to a home-made moving stage to minimize photodamage. All experiments were carried out at room temperature.

Received: April 10, 2008
Revised: May 31, 2008
Published online: August 1, 2008

[1] a) C. Goh, J. Kline, M. D. McGehee, E. N. Kadnikova, M. J. Fréchet, *Appl. Phys. Lett.* **2005**, *86*, 122110. b) D. Braun, G. Gustafsson, D. McBranch, A. J. Heeger, *J. Appl. Phys.* **1992**, *72*, 564. c) P. Dyreklev, M. Berggren, O. Inganäs, M. R. Andersson, O. Wennerström, T. Hjertberg, *Adv. Mater.* **1995**, *7*, 43. d) T.-W. Lee, *Adv. Funct. Mater.* **2007**, *17*, 3128. e) T.-W. Lee, Y. Chung, O. Kwon, J.-J. Park, *Adv. Funct. Mater.* **2007**, *17*, 390.

[2] a) Y. D. Park, D. H. Kim, J. A. Lim, J. H. Cho, Y. Jang, W. H. Lee, J. H. Park, K. Cho, *J. Phys. Chem.* **2008**, *112*, 1705. b) I. McCulloch, C. Bailey, M. Giles, M. Heeney, I. Love, M. Shkunov, D. Sparrowe, S. Tierney, *Chem. Mater.* **2005**, *17*, 1381. c) B. S. Ong, Y. Wu, P. Liu, S. Gardner, *Adv. Mater.* **2005**, *17*, 1141. d) H. Yang, T. J. Shin, L. Yang, K. Cho, C. Y. Ryu, Z. Bao, *Adv. Funct. Mater.* **2005**, *15*, 671.

[3] a) M. C. Scharber, D. Mühlbacher, M. Koppe, P. Denk, C. Waldauf, A. J. Heeger, C. J. Brabec, *Adv. Mater.* **2006**, *18*, 789. b) C. L. Chochos, S. P. Economopoulos, V. Deimede, V. G. Gregoriou, M. T. Lloyd, G. G. Malliaras, J. K. Kallitsis, *J. Phys. Chem. C* **2007**, *111*, 10732. c) F.-C. Chen, Y.-K. Lin, C.-J. Ko, *Appl. Phys. Lett.* **2008**, *92*, 023307.

[4] a) B. Li, G. Sauvé, M. C. Lovu, M. Jeffries,-EL R. Zhang, J. Cooper, S. Santhanam, L. Schultz, J. C. Revelli, A. G. Kusne, T. Kowalewski, J. L. Snyder, L. E. Weiss, G. K. Fedder, R. C. McCullough, D. N. Lambeth, *Nano Lett.* **2006**, *6*, 1598. b) K. P. R. Nilsson, O. Inganäa, *Nat. Mater.* **2003**, *2*, 419. c) Y. Tang, F. He, M. Yu, F. Feng, L. An, H. Sun, S. Wang, Y. Li, D. Zhu, *Macromol. Rapid Commun.* **2006**, *27*, 389. d) C. Li, M. Numata, M. Takeuchi, S. Shinkai, *Angew. Chem. Int. Ed.* **2005**, *44*, 6371.

[5] I. F. Perepichka, D. F. Perepichka, H. Meng, F. Wudl, *Adv. Mater.* **2005**, *17*, 2281.

[6] N. C. Greenham, I. D. W. Samuel, G. R. Hayes, R. T. Phillips, Y. A. R. R. Kessener, S. C. Moratti, A. B. Holmes, R. H. Friend, *Chem. Phys. Lett.* **1995**, *241*, 89.

[7] H. Saadeh, T. Goodson, III, L. Yu, *Macromolecules* **1997**, *30*, 4608.

[8] a) J. Y. Kim, K. Lee, N. E. Coates, D. Moses, T.-Q. Nguyen, M. Dante, A. J. Heeger, *Science* **2007**, *317*, 222. b) W. Ma, C. Yang, X. Gong, K. Lee, A. J. Heeger, *Adv. Funct. Mater.* **2005**, *15*, 1617.

[9] D. Mühlbacher, M. Scharber, M. Morana, Z. Zhu, D. Waller, R. Gaudiana, C. Brabec, *Adv. Mater.* **2006**, *18*, 2884.

[10] a) W. Wang, K. A. S. Fernando, Y. Lin, M. J. Meziani, L. M. Veca, L. Cao, P. Zhang, M. M. Kimani, Y.-P. Sun, *J. Am. Chem. Soc.* **2008**, *130*, 1415. b) T. J. Savenije, J. E. Kroeze, X. Yang, J. Loos, *Adv. Funct. Mater.* **2005**, *15*, 1260. c) Q. Zhang, T. P. Russell, T. Emrick, *Chem. Mater.* **2007**, *19*, 3712. d) K. Matsumoto, M. Fujitsuka, T. Sato, S. Onodera, O. Ito, *J. Phys. Chem. B* **2000**, *104*, 11632. e) I.-W. Hwang, D. Moses, A. J. Heeger, *J. Phys. Chem. C* **2008**, *112*, 4350.

[11] a) G. Yu, J. Gao, J. C. Hummelen, F. Wudl, A. J. Heeger, *Science* **1995**, *270*, 1789. b) G. Li, V. Shrotriya, J. Huang, Y. Yao, T. Moriarty, K. Emery, Y. Yang, *Nat. Mater.* **2005**, *4*, 864. c) W. U. Huynh, J. J. Dittmer, A. P. Alivisatos, *Science* **2002**, *295*, 2425. d) A. G. Manoj, A. A. Alagiriswamy, K. S. Narayan, *J. Appl. Phys.* **2003**, *94*, 4088.

[12] a) J. Geng, T. Zeng, *J. Am. Chem. Soc.* **2006**, *128*, 16827. b) E. Kymakis, G. A. J. Amaratunga, *Appl. Phys. Lett.* **2002**, *80*, 112. c) E. Kymakis, I. Alexandrou, G. A. J. Amaratunga, *J. Appl. Phys.* **2003**, *93*, 1764. d) B. J. Landi, R. P. Raffaelle, S. L. Castro, S. G. Bailey, *Prog. Photovolt.: Res. Appl.* **2005**, *13*, 165. e) B. J. Landia, S. L. Castrob, H. J. Rufa, C. M. Evansa, S. G. Baileyc, R. P. Raffaelle, *Sol. Energy Mater. Sol. Cells* **2005**, *87*, 733. f) S.-H. Hur, D.-Y. Khang, C. Kocabas, J. A. Roger, *Appl. Phys. Lett.* **2004**, *85*, 5730.

[13] M. J. O'Connell, in: *Carbon Nanotubes: Properties and Applications*, Taylor and Francis, Boca Raton, FL **2006**, pp. 153–186.

[14] A. Ikeda, K. Nobusawa, T. Hamano, J.-I. Kikuchi, *Org. Lett.* **2006**, *8*, 5489.

[15] a) A. B. Dalton, C. Stephan, J. N. Coleman, B. McCarthy, P. M. Ajayan, S. Lefrant, P. Bernier, W. J. Blau, H. J. Byrne, *J. Phys. Chem. B* **2000**, *104*, 10012. b) J. N. Coleman, A. B. Dalton, S. Curran, A. Rubio, A. P. Davey, A. Crury, B. McCarthy, B. Lahr, P. M. Ajayan, S. Toth, R. C. Barklie, W. J. Blau, *Adv. Mater.* **2000**, *12*, 213. c) A. Star, J. F. Stoddart, D. Steuerman, M. Diehl, A. Boukai, E. W. Wong, X. Yang, S.-W. Chung, H. Choi, J. R. Heath, *Angew. Chem. Int. Ed.* **2001**, *40*, 1721.

[16] a) W. Z. Yuan, J. Z. Sun, Y. Dong, M. Häussler, F. Yang, H. P. Xu, A. Qin, J. W. Y. Lam, Q. Zheng, B. Z. Tang, *Macromolecules* **2006**, *39*, 8011. b) W. Z. Yuan, Y. Mao, H. Zhao, J. Z. Sun, H. P. Xu, J. K. Jin, Q. Zheng, B. Z. Tang, *Macromolecules* **2008**, *41*, 701.

[17] A. G. Ryabenko, T. V. Dorofeeva, G. I. Zvereva, *Carbon* **2004**, *42*, 1523.

[18] J. Chen, H. Liu, W. A. Weimer, M. D. Halls, D. H. Waldeck, G. C. Walker, *J. Am. Chem. Soc.* **2002**, *124*, 9034.

[19] T.-A. Chen, X. Wu, R. D. Rieke, *J. Am. Chem. Soc.* **1995**, *117*, 233.

[20] a) B. Valeur, in: *Molecular Fluorescence Principles and Applications*, Wiley-VCH, Weinheim, Gemany **2002**, pp. 72–124. b) M. E. Ei-Zaria, A. R. Genady, *Appl. Organomet. Chem.* **2007**, *21*, 983.

[21] B. Kraabel, D. Moses, A. J. Heeger, *J. Chem. Phys.* **1995**, *103*, 5102.

[22] a) M. Theander, A. Yartsev, D. Zigmantas, V. Sundström, W. Mammo, M. R. Andersson, O. Inganäs, *Phys. Rev. B* **2000**, *61*, 12957. b) A. S. D. Sandanayaka, Y. Takaguchi, T. Uchida, Y. Sako, Y. Morimoto, Y. Araki, O. Ito, *Chem. Lett.* **2006**, 1188. c) V. Biju, T. Itoh, Y. Baba, M. Ishikawa, *J. Phys. Chem. B* **2006**, *110*, 26068.

[23] I. W. Chiang, B. E. Brinson, A. Y. Huang, P. A. Willis, M. J. Bronikowski, J. L. Margrave, R. E. Smalley, R. H. Hauge, *J. Phys. Chem. B* **2001**, *105*, 8297.

[24] a) K. J. Ziegler, Z. Gu, H. Peng, E. L. Flor, R. H. Hauge, R. E. Smalley, *J. Am. Chem. Soc.* **2005**, *127*, 1541. b) G. A. Forrest, A. J. Alexander, *J. Phys. Chem. C* **2007**, *111*, 10792.

